

Growth and collapse of the 2018–2019 lava dome of Merapi volcano

Karim Kelfoun, Agus Budi Santoso, Thierry Latchimy, Martial Bontemps, Ilham Nurdien, François Beauducel, Ali Fahmi, Raditya Putra, Nabil Dahamna, Antoine Laurin, et al.

▶ **To cite this version:**

Karim Kelfoun, Agus Budi Santoso, Thierry Latchimy, Martial Bontemps, Ilham Nurdien, et al.. Growth and collapse of the 2018–2019 lava dome of Merapi volcano. Bulletin of Volcanology, 2021, 83 (2), 10.1007/s00445-020-01428-x . hal-03118291

HAL Id: hal-03118291
https://uca.hal.science/hal-03118291

Submitted on 22 Jan 2021

HAL is a multi-disciplinary open access archive for the deposit and dissemination of scientific research documents, whether they are published or not. The documents may come from teaching and research institutions in France or abroad, or from public or private research centers.

L'archive ouverte pluridisciplinaire **HAL**, est destinée au dépôt et à la diffusion de documents scientifiques de niveau recherche, publiés ou non, émanant des établissements d'enseignement et de recherche français ou étrangers, des laboratoires publics ou privés.



Distributed under a Creative Commons Attribution 4.0 International License

Growth and collapse of the 2018−2019 lava dome of Merapi volcano.

Published in **Bulletin of Volcanology, Springer Nature, 2021**

DOI: 10.1007/s00445-020-01428-x BUVO-D-20-00060R3

Karim Kelfoun[1], Agus Budi Santoso[2], Thierry Latchimy[3], Martial Bontemps[3], Ilham Nurdien[2], François Beauducel[4,5], Ali Fahmi[5], Raditya Putra[2], Nabil Dahamna[5], Antoine Laurin[5], Mochammad Husni Rizal[5], Jatmika Teja Sukmana[5], Valentin Gueugneau[1]

1. Université Clermont Auvergne, CNRS, IRD, OPGC, Laboratoire Magmas et Volcans, Clermont-Ferrand, France.
2. Center for Volcanology and Geological Hazard Mitigation, Jalan Cendana 15, Yogyakarta, Indonesia
3. Université Clermont Auvergne, Observatoire de Physique du Globe de Clermont-Ferrand, Clermont-Ferrand, France.
4. Université de Paris, Institut de physique du globe de Paris, CNRS, Paris, France
5. Université Grenoble Alpes, Université Savoie Mont Blanc, CNRS, IRD, IFSTTAR, ISTerre, Grenoble, France

Abstract

Lava dome collapses are a major threat to the population living near such volcanoes. However, it is not possible to forecast collapses reliably because the mechanisms are not clearly understood, due partly to the lack of continuous observations of such events. To address this need for field data, we have developed new monitoring stations, which are adapted to the volcanic environment. The stations tracked the complete evolution of the 2018−2019 lava dome of Merapi volcano (Indonesia) and the associated pyroclastic density currents. During the fourteen months of activity, the stations acquired thermal, high-resolution visual images and movies in stereoscopic configurations. The dome developed on a plateau flanked by steep sides (~40°−50°) inside the crater, which was open to the SE. We observed that the dome behaved in a viscous manner (with a viscosity of 10^9 Pa s for the interior to 10^{13} Pa s for external parts of the dome) on gentle slopes, and in a brittle way (friction angle ~35°, cohesion <100 kPa) on slopes steeper than 35°. Thus, the lava dome was unable to grow on the outer slopes of the plateau and a significant volume of lava ($350−750×10^3$ m^3) accumulated and collapsed daily to the SE in relatively small volumes (<10 000 m^3), preventing the lava dome from reaching the critical volume necessary for pyroclastic density currents to form and threaten the surrounding population. The cause of the small and frequent collapses was purely gravitational during the dome activity. This suggests that relatively small differences in the summit morphology can control dome evolution, favouring either a lava dome restricted to a small volume and leading to only a minor crisis, or more voluminous dome growth and a catastrophic collapse.

Introduction

Lava domes are formed by the extrusion and the accumulation of viscous lava above a vent. Their destruction can generate pyroclastic density currents (PDCs) that can devastate villages and infrastructure, and are a major threat to the surrounding population. Predicting the characteristics of PDCs formed by a lava dome is crucial for risk and hazard assessment. Several questions remain unanswered concerning the growth and destruction of lava domes. In terms of hazard assessment, the question of what causes the destruction of the lava dome remains. Is it purely gravitational and caused by over-steepening of the dome (Swanson et al., 1987)? Is the pressure of volcanic gases responsible for dome destruction (Sparks, 1997; Voight and Elsworth, 2000)? What are the effects of rainfall (Carn et al., 2004; Taron et al., 2007) and of the structure of the dome and its substratum (Voight et al., 2000a)? What is the relationship between the dome's characteristics and those of associated PDCs (Kelfoun et al., 2017)? It is not easy to answer these questions as multiple phenomena can be involved, and may vary from one dome collapse to another. Over the last few years, increasingly sophisticated models of domes and PDCs have been developed to address this issue (Hale, 2008; Husain et al., 2014; Kelfoun et al. 2017; Harnett et al. 2018). One difficulty in developing models is the lack of data on real phenomena with which to compare the models objectively in order to determine what they are able to predict successfully and which conditions they can be applied to. The highly dangerous nature of this volcanic activity, difficulty of access to the crater areas, and the suddenness of destabilisation phases, explain the lack of observations. The morphology of Merapi volcano that was created after the 2010 eruption is good for observing the emplacement of lava domes and for acquiring the observation data needed. We took advantage of this to develop and install new monitoring stations dedicated to continuous and real-

time monitoring observation of lava domes. This paper presents the system we developed, and the results of more than one year's monitoring of the lava dome and its destabilisations. All the images recorded are referenced in a database which is accessible online. The data give a clear view of the conditions for dome stability, the cause of destruction and the origin of the PDCs. Combined with stress equilibrium equations and numerical models, we estimate the mechanical behaviour of the lava dome and its variations in space and time.

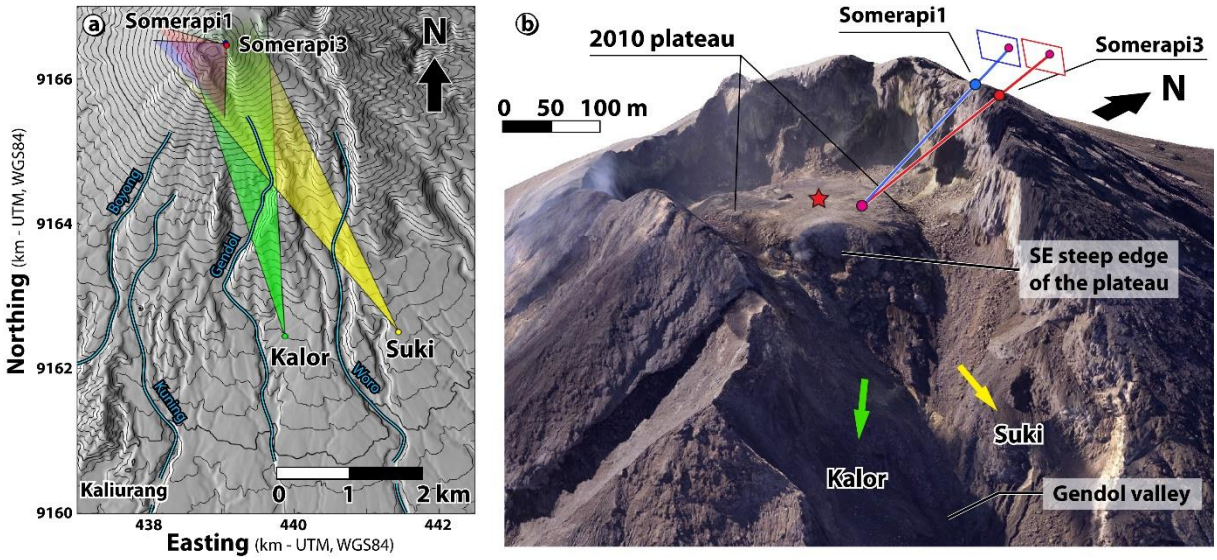


Fig. 1 (a) Location of the four monitoring stations at Merapi volcano and the Gendol river. (b) 3D view of the summit before the birth of the dome, with the locations of the summit monitoring stations. The red and blue lines indicate how a point is localized in 3D by stereophotogrammetry. The red star indicates the vent location of the 2018 lava dome

Activity at Merapi volcano is generally characterised by lava domes that grow at the summit and explode or collapse, forming PDCs. Generally, these PDCs are several kilometres long (6.5 km in 1994, Abdurachman et al., 2000; 6 km in 1998, Schwartzkopf et al., 2005; 7 km in 2006, Charbonnier and Gertisser, 2008) and they are formed by pyroclastic flows concentrated in the valleys, often associated with dilute surges, that destroy the interfluves. Merapi is very active, with an average interval between dome growth of about 4 to 6 years over the last century. The most recent dome destructions occurred in 1992, 1994, 1997, 1998 and 2006. Less frequently, the eruptions are larger and more destructive: these can destroy part of the summit, and PDCs can reach up to 15 km, as occurred in 1930 and 2010 (Voight et al., 2000a; Komorowski et al., 2013). Even greater eruptions caused the destruction of the entire summit cone of the volcano in the 19th century. A complete and detailed summary of Merapi's activity up to 1998, as well as relevant references, can be found in Voight et al. (2000a) and Newhall et al. (2000). Together with the regularity of the successive eruptive phases, Merapi volcano is also characterised by a more or less constant effusion rate over long time periods. According to Siswowidjoyo et al. (1995), the long term effusion rate between 1890 and 1992 is about 100 000 m^3/month, i.e. 3000−3500 m^3/day. This long term rate hides a marked contrast between the null effusion rate during quiescence phases (lasting a few years) and the very high rates during eruptive episodes (days to months). The effusion rate was estimated at 6 million m^3/month (i.e. 200 000 m^3/day) during the paroxysmal eruption of 1930 (Siswowidjoyo et al., 1995). The 1992 lava dome begun by a effusion rate of 200 000 m^3/day in February, reached a volume of 9.1 million m^3 and remained stable. For the 1994 lava dome, the effusion rate started at 6500 m^3 / day and culminated in 17 000 m^3/day, three months later (Ratdomopurbo and Poupinet, 2000). This relatively low rate, compared to the other recent domes, does not necessarily mean a reduced hazard. The lava of the 1994 dome accumulated over nine months,

forming a lava dome 50 m thick, with a volume of 2.6 million m^3, which collapsed in November 1994, devastating two villages and killing more than 60 people. The collapse was not explosive and, despite the PDCs destroying villages over 6 km from the summit, the scientists working at the summit only about 100 m from the dome were not injured (Voight et al, 2000b). In 2006, a dome reached a total volume of about 5.3 million m^3 in 38 days with a maximum effusion rate of 285 000 m^3/day (Ratdomopurbo et *al*, 2013). During the paroxysmal eruption in 2010, a huge rate of ~ 25 m^3/s (i.e. 2 million m^3/day) was estimated by Pallister et al. (2013) but this was sustained for only a few days (29 Oct−4 Nov), before the dome and summit explosions on 5 November 2010.

Today, one of the main problems faced by the Merapi Observatory is to predict whether the lava extrusion will pose a threat to the surrounding population. Despite intense activity and several decades of observation, there is currently no clear answer. The 2018−2019 lava dome grew up on a morphology that was shaped by the 2010 eruption: successive explosions and collapses destroyed the 2010 summit to create a 200 m-deep crater open to the SE (Fig. 1). A lava dome, 200 m in diameter and 40 m high, grew and solidified at the bottom of the crater, marking the end of the 2010 eruption. The surface of the 2010 dome is relatively flat and will be referred to here as the plateau. The edges of this plateau are relatively steep (40°−50°), the SE edge coinciding with the crater edge and overhanging the SE flank and the Gendol valley (Fig. 1). Between 2012 and 2014, six explosions created a major open fissure (Darmawan et al, 2018), referred to here as the summit fissure. It is oriented NW-SE and splits the plateau in two. A detailed analysis of the pre-eruptive topography is given in Darmawan et al. (2018).

Monitoring system

Dome activity is often monitored by its seismicity. Although this method has many advantages, interpretation of dome activity is difficult. Visual and thermal observations have already been carried out on lava domes (e.g. Major et al, 2009, at Mount St Helens; Diefenbach et al, 2013, at Redoubt; Walter at al., 2013, at Merapi; Nakada et al., 2019 at Sinabung). However, one difficulty in studying the mechanisms of collapse and PDC genesis is the suddenness of these events. Videos that show the dynamics of a dome collapse and the initiation of PDCs clearly, as first published by Sato et al. (1992) for Unzen volcano, are scarce.

Our system is designed to make long-term, continuous and real time (< 1 min) observations of volcanic activity. It is composed of four monitoring stations, two on the flanks at ~5 km from the summit and two at the summit (Fig. 1), connected to observatories and research laboratories by a Wi-Fi network deployed on the flank of the volcano. The stations were installed in 2014, i.e. well before the 2018−2019 eruption, and they captured the entire dome emplacement. Each station contains a high-resolution digital single lens reflex (DSLR) camera (Canon, EOS 2000D) and one or two webcams. The advantage of a DSLR camera is the quality of the lens and the long exposure time that allows high quality pictures to be taken, even at night. Two stations (Somerapi1 and Suki, Fig. 1) are also equipped with a thermal camera (Optris, PI400) that captures an image every 3 minutes. The temperature range of the cameras was set to 0−250°C. In this range, the camera sensibility is less than 0.1°C and the temperature precision of the summit camera is better than 2°C in the absence of clouds or plumes. Higher initial temperatures (up to 800°C) were estimated by the extrapolation of the temperature variations. For example, blocks that detach show an exponential cooling that can be extrapolated backward to estimate the initial block temperature with an accuracy of some tens of °C. Fitting the temperature gradients along a detachment surface with a model of thermal conduction (see section Thermal properties) gives the interior temperature of the dome with a similar accuracy. Each station is independent in terms of energy supply, with the power provided by solar panels. Each station is controlled by a microcomputer (Raspberry PI 3). It is set to acquire data automatically but it is also possible to change the programming remotely, and data can be acquired at any time. The stations can receive signals following seismic analysis carried out automatically at the observatory, which triggers movie recordings. They can also trigger movies from their own analysis of the webcam images. A buffer of one minute allows the onset of the event to be captured without loss of information. To save bandwidth, the more voluminous data can be saved in the

stations and downloaded later. All the visible and thermal images acquired during the dome growth are available online: http://wwwobs.univ-bpclermont.fr/SO/televolc/stereovolc/data/domerapi/Merapi.html

Stations are installed in stereoscopic geometries to spatially locate each identified object on two images (Fig. 1b), following the method and codes presented in Kelfoun et al (2020). The resolution of the digital cameras at the dome is about 4−5 cm for the summit stations and 12−19 cm for the flank stations. The system allows the topography of the observed areas and their evolution to be calculated over time. By comparing photographs taken at various times, it is possible to reconstruct the trajectories and velocities of the observed objects in 3D (refer to Kelfoun et al, 2020, for details of the method used). Often, however, one (or more) station was down and stereoscopy was not available. The locations, distances and velocities can be estimated using parallax between visible and thermal images, by projections onto previously calculated topographies or by using previously calculated pixel sizes. Our interpretations are also based on other data, when available, such as seismic records, meteorological records, drone surveys and video images from the Merapi Observatory, as well as topographies calculated by the structure from motion method using several pictures taken from the crater during trips for routine system maintenance.

Results

The 2018−2019 eruptive crisis began with two explosions, on 11 May and 1 June 2018, preceded by clear emissions of hot gases from the summit fissure. The new dome appeared in August from the summit fissure. Movies of the whole dome growth, recorded by the summit cameras, is given in Online Resource 1 (thermal) and 2 (visible). The growth can be divided into three phases (Fig. 2).

Phase 1: radial growth (10−28 August 2018)

The magma was very close to the surface on 10 August 2018, as shown by the temperature increase in the summit fissure. On 12 August, it was observed by a monitoring drone of Merapi Observatory (BPPTKG, *Balai Penyelidikan dan Pengembangan Teknologi Kebencanaan Geologi*) in the summit fissure (Global Volcanism Program, 2019a). The exact date of the onset of dome extrusion is not known because of a data transmission problem over this period. On 18 August, when the problem had been resolved, the dome was already protruding from the fissure. It was ~6 m thick above the mean elevation of the 2010 plateau, and 40 m wide and 70 m long in the SE-NW direction of the fissure.

In this paper, the dome front refers to the boundary of the massive lava rather than the talus (Fig. 2d). Because the spreading is initially radial, the front is circular and several front velocities can be measured. The outer boundary of the talus deposits, in contact with the underlying rocks, is called the front of the talus.

During the first two weeks, the mean horizontal velocity of the dome front was 1 to 2 m/day to the north-west, the north-east and the south-east (it was not possible to observe the south-west part with our network) with maximal velocities of 4 m/day (Fig. 3a). Fluctuations in velocity were due to the dome progressing by destabilization of the blocks on the dome surface at the front (the largest blocks being 20 m wide and 5 m high) where the slope became too steep. Thus, the front of the dome progressed incrementally, some parts remaining static for hours or days and then progressing almost instantaneously by a few meters when a destabilization occurred. The horizontal velocity of blocks at the surface of the dome was slightly higher than the front velocity, at 1 to 3 m/day. Block were extruded and broken up, each with a specific velocity, making difficult the measurement of an accurate and representative dome surface velocity. The dome thickened vertically at a velocity that decreased from 1.5 m/day on 18 August to 0.25 m/day on 28 August (Fig. 3b). The evolution of the dome volume gives an initial effusion rate of about 5500 m^3/day.

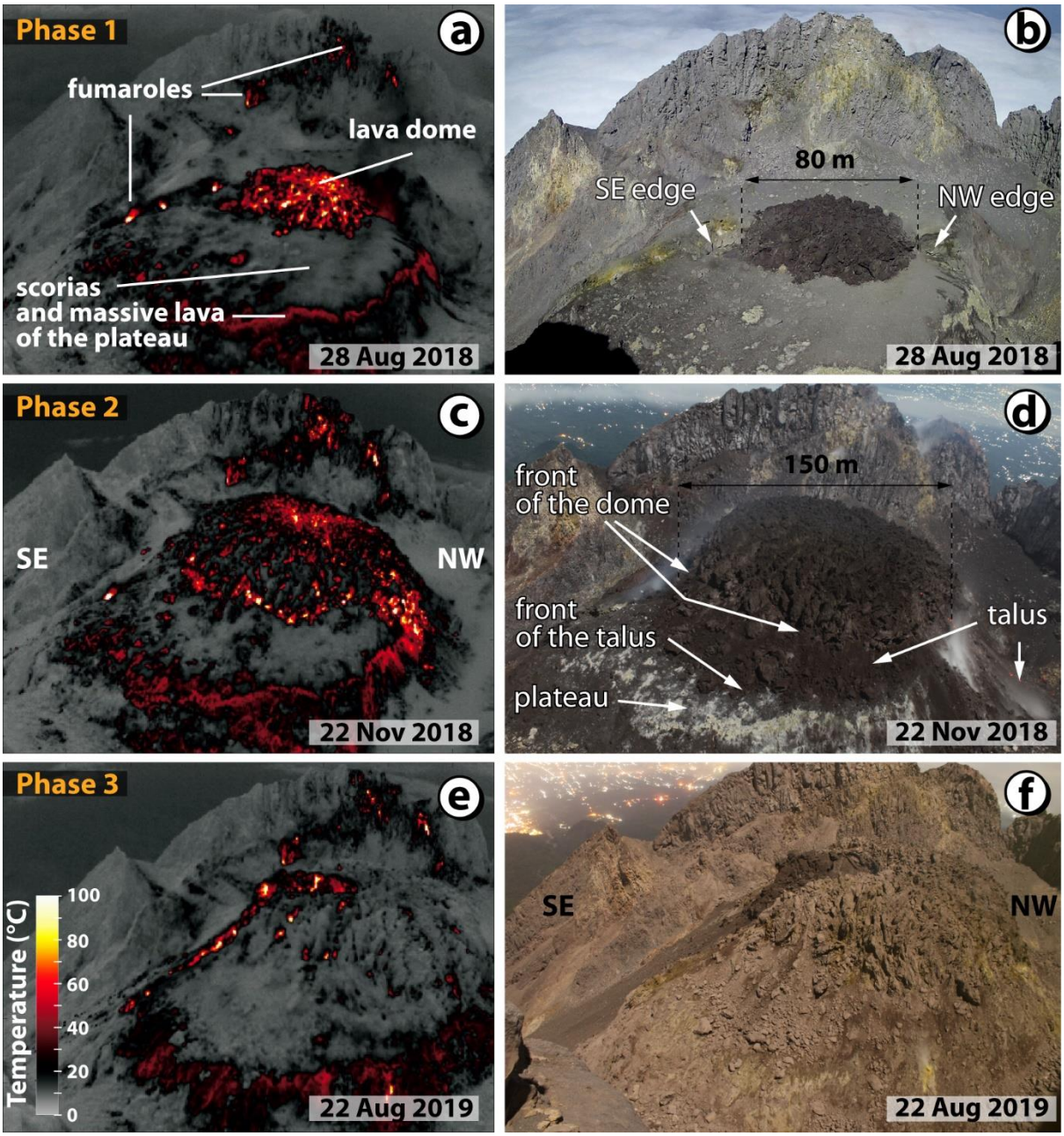


Fig. 2 The three stages of the 2018−2019 lava dome growth at Merapi volcano. Left: thermal images. Right: visible images. The growth was initially radial (during phase 1, a−b), then it became asymmetric to the NW (phase 2, c−d) before forming a flow oriented to the SE (phase 3, e−f). See Online Resource 1 and 2 for a complete movie of the 14 months of growth. All the images recorded are available at the following link: *http://wwwobs.univ-bpclermont.fr/SO/televolc/stereovolc/data/domerapi/Merapi.html*

Initially, the volume of rocks accumulated ahead of the dome front by block destabilisations was relatively low and no talus was observed before the end of August. The temperatures of the dome surface were relatively cold, between 20°C for the large blocks and 200°C in fissures that formed in extensional areas, with a mean value of about 50°C. Where blocks detached, we were able to estimate the temperature of the dome interior of about 300°C at 2−3 m below the surface and about 500°C at a depth of 5 meters, by extrapolating backward the cooling evolution.

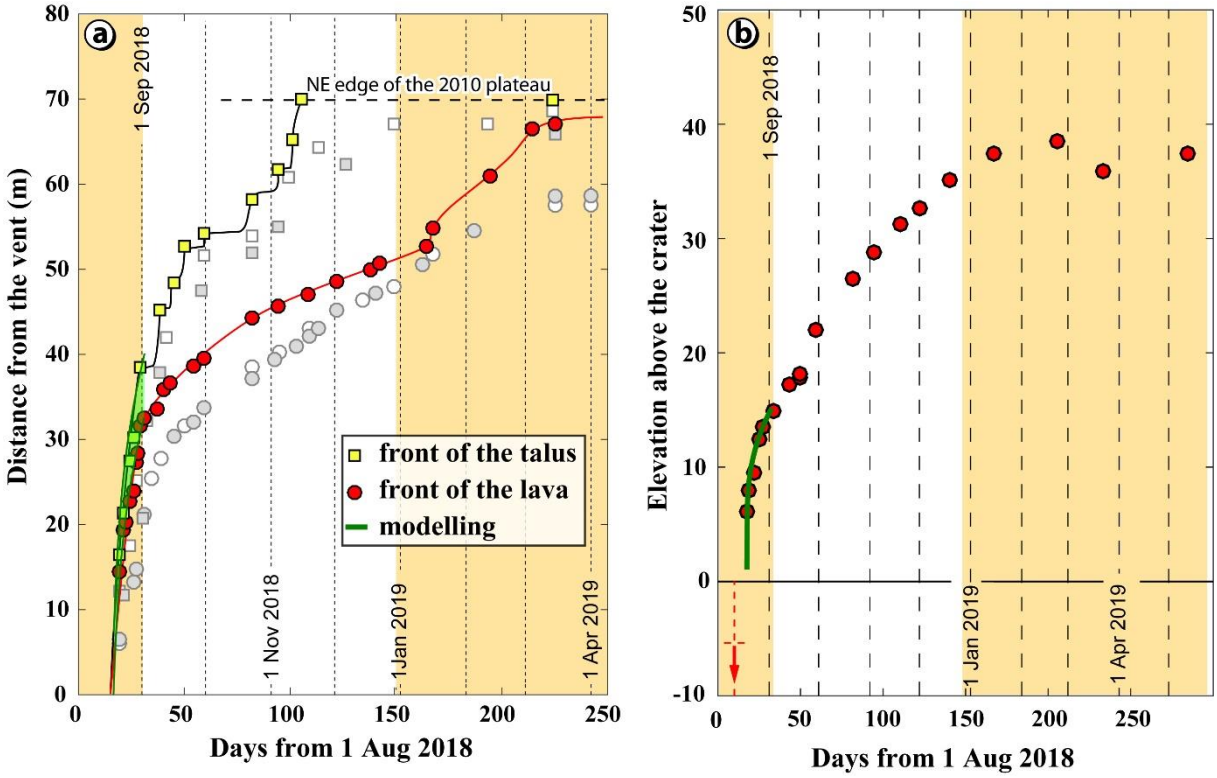


Fig. 3 (a) Location of the fronts of the talus (squares) and of the massive lava (circles) of the 2018−2019 lava dome over time. The locations are measured in the direction of the summit stations (N55) and of the NE edge of the plateau. Grey and white symbols are measurements to close directions (N50 and N60) to show the variability of the dome's progression. The stepped aspect of the talus curve is explained by the front progression by surface destabilisations. (b) Dome thickness with time. The red arrow indicates that the lava was lower than -6 m in the summit fissure on 10 August 2018. For both parts of the figure, the background colours identify the three phases: radial growth, anisotropic growth and oriented growth. The green lines are the results of the numerical modelling (see section on 'Viscosity')

Phase 2: anisotropic growth (September – December 2018)

On 28 August 2018, the dome reached the NW edge of the plateau (Fig. 2b) and began to collapse, forming hot rock falls that accumulated progressively in the depression below the plateau as a talus of blocks and ash (Fig. 2c−d). The term collapse is used here to describe a gravitational destabilization that affects the internal massive lava of the dome and not just the blocks at the surface, regardless of the volume destabilized. It ranges from small destabilisations, sometimes called crumbling (Sato et al., 1992), to a destabilization affecting the entire dome. Up to November, the talus did not affect the dome's behaviour because it was not significant in thickness relative to the size of the plateau. During this stage, the lava forming the dome was able to flow and collapse at the NW edge, creating a preferential flow direction. For example, on 28 September, the surface velocities were 1.5−1.8 m/day in the NW sector while they were about 1 m/day in other directions. By October, the dome was thicker and collapsing blocks were about 15 m wide and 5−10 m high. The internal temperature of the dome could be measured where collapses occurred, giving a value of about 50°C at the surface, with an increase of 70°C/m, vertically, towards the interior of the dome.

On the plateau, the radial velocities decreased progressively with time due to the preferential orientation of the lava flow to the NW edge but also due to the increase in dome radius, together with a decrease in effusion rate (see sections below). Because of the velocity decrease, it took more time for the lava on the plateau to reach the front. This caused the crust to thicken, leading to larger volume collapses at the

front. A clear talus was observed at the NE side of the plateau in September, distinguishable from the lava by its cooler temperature, its morphology and its texture. The presence of the talus slowed the dome down even more, thus increasing the thickness of the talus. The slope of the dome front reached an angle of 50° to 60° (higher locally) before collapses occurred. The dome was stable on the interior slope of the talus but was unable to grow on its 35° exterior slope (Fig. 4). Thus, the dome progressed either by sliding over the talus or by the constant destabilisations at its front, which increased the width of the talus and moved the boundary between the interior and the exterior slopes outwards.

During phase 2, as the dome thickened, its morphology changed and it developed a clear central depression, some meters in depth, above the vent. As shown in Fig. 2c, the central depression was hotter than the rest of the dome surface (except at the front where collapses occurred).

Phase 3: oriented flux (January – September 2019)

The active lava dome grew slowly towards the SE edge of the plateau (i.e. the solidified 2010 dome), which it reached in November 2018, about 100 days after onset of extrusion (mean velocity of 70 cm/day). As at the NW edge, the blocky front was pushed outwards from the plateau, enabling the lava to flow more easily. However, given the opening to the SE, the blocks and ash fell from the summit cone of Merapi down into the Gendol valley rather than accumulating. Meanwhile, to the NW side, the talus became thick enough to influence the emplacement. Flow movement in this south-easterly direction was easier, which explains why the velocities of the dome surface and the lava flux increased progressively (Fig. 5) in the SE sector. Lava collapses became increasingly common and the first PDCs were observed. On 28 December, dome growth was still radial, albeit asymmetric. In January, the surface temperature and the displacements showed that the lava flow was mostly directed to the SE and that the dome was becoming decreasingly mobile in all other directions. By 1 March 2019, the lava was flowing only within a sector of 60° from the vent to the SE (Fig. 4). In this sector, the surface velocity of the blocks on the dome surface had increased progressively from less than 2 m/day in November 2018 to ~4 m/day in March 2019 (Fig. 5). Elsewhere, the dome was nearly static and its morphology underwent no further significant change. The dome surface was cut by radial faults which separated large sectors (~60°) that moved slowly as rigid blocks. Mean displacement for these sectors over a several-week period was about 6 cm/day in March 2019, 4 cm/day in June 2019, less than 3 cm/day in August 2019 and 2 cm/day in September 2019.

The stations on the flanks (Kalor and Suki, Fig. 1) provided an opportunity to observe the internal structure of the dome when it collapsed in the SE sector. The dome was composed of two parts (see additional figures, Online Resource 3): an 11- to 14-m-thick crust, and the internal massive lava, which was up to 20 m thick. The crust was cut vertically into pseudo-columns (~5 m wide) and formed a near-vertical cliff facing the SE flank. The crust itself could be divided into two parts separated by a crude but visible discontinuity. In the upper 5−7 m no glow was seen, whereas in the lower, ~8-m-thick part, hot lava was observed at night during collapse events (with long exposure photos, >60 s). Below the crust, the surface slope of the hot massive lava was about 30−40°.

Between December 2018 and September 2019, the volume of the lava dome remained roughly constant, even though the magma flux was still high. This was because the volume lost through dome collapse balanced the lava supply. The only slight change to the dome morphology was in the active sector, where the surface morphology evolved from rounded to angular in profile. The collapse mechanism remained similar during this 10-month period: the lava flowed to the SE, at the edge of the 40°−50° slope overhanging the SE flank. Since the surface moved faster than the base, the slope at its front increased up to the point where it became unstable. Two sorts of collapse were observed; in the most common, the top of the block tilted faster than the base and the cameras captured an anti-clockwise rotation of the blocks (Fig. 6). This mechanism is similar to the collapses described by Sato et al, 1992, for the dacite lava dome of Unzen volcano. The other destabilization resembled a sliding motion, with the base moving faster than the top, and the block undergoing a clockwise movement (see the dome front, Fig. 4). Each

collapse involved a volume of some thousands of cubic meters, a few meters in thickness and 10 to 40 meters in length and width (Fig. 6). Typically, this destabilisation activity led to a slope increase lasting some days, followed by a series of collapses once the slope was steep enough. All the PDCs detected were purely gravitational and no associated explosions were observed during the nine months of the collapse activity.

From June 2019, the velocity of the blocks at the surface of the SE sector decreased progressively (Fig. 5). In September 2019, the crust of the active part thickened, forming larger, whaleback-shaped slabs. At the back of the dome, between the active lava (moving at less than 1 m/day) and the non-mobile part, shearing created a series of three linear sectors of nested slabs a few meters wide and 2 m thick (movie in Online Resource 4). The slabs closest to the lava move faster (10 cm/day) than the others (<1 cm/day). Similar slabs were observed on previous domes as well as in cross section for the 1994 lava dome (see Online Resource 3).

End of the activity

At 11:36 (local time) on 22 September 2019, an explosion occurred from a SE-NW fracture located directly above the summit fissure. Cracks opened in the active and solidified parts of the dome. Hot degassing from the active lava lobe was recorded by the thermal camera at the summit. An ash plume rose around 800 m above the summit and PDCs were detected (Global Volcanism Program, 2019a). This explosion was accompanied by an abrupt deflation of the SE part of both the active and the solidified lava dome. From the time steps of the thermal images this took place in less than 3 minutes, and perhaps as little as a few seconds. The vertical deflation measured from stereoscopic reconstruction reached 2 m directly above the vent and 80 cm to 1 m elsewhere (Online Resource 3). No significant destruction of the dome was observed after the explosion and the PDCs recorded were probably caused by instabilities, such as those seen from December 2018. After this explosion, the dome solidified throughout and only very localized displacements were recorded subsequently. No more glowing was observed at the summit after the explosion.

On 14 October, at 16:31 (local time), a more powerful eruptive event, which lasted 4 min 30 s, generated an ash plume that reached 3 km above the summit and PDCs that travelled down the SE flank (Global Volcanism Program, 2019b). The majority of the dome that had deflated on 22 September was destroyed in this eruption, together with the monitoring stations at the summit. The stations on the flank continued recording, and showed that this explosion caused a displacement of the SE part of the plateau (an area of about 50 m high and 100 m wide) of 2 m to the SE.

Other explosions were observed on 9 November 2019, 17 November 2019 and 13 February 2020. On 3 March 2020, at 5:29 AM (local time) another strong explosion occurred, with a jet emitted from each side of the dome (NE and SW), originating from a NE-SW fault opened beneath it (and perpendicular to the summit fissure). Other explosions occurred on 27, 28 March, 10 April and 21 June 2020. This series of explosions almost completely destroyed the SE part of the 2018−2019 lava dome.

Discussion

In this section, our observation data are compared with stress equilibrium equations, with numerical solutions of mechanical and thermal equations, and with simulations of dome emplacement to estimate the properties of the lava dome. All the codes and the input parameters are available in Online Resource 5.

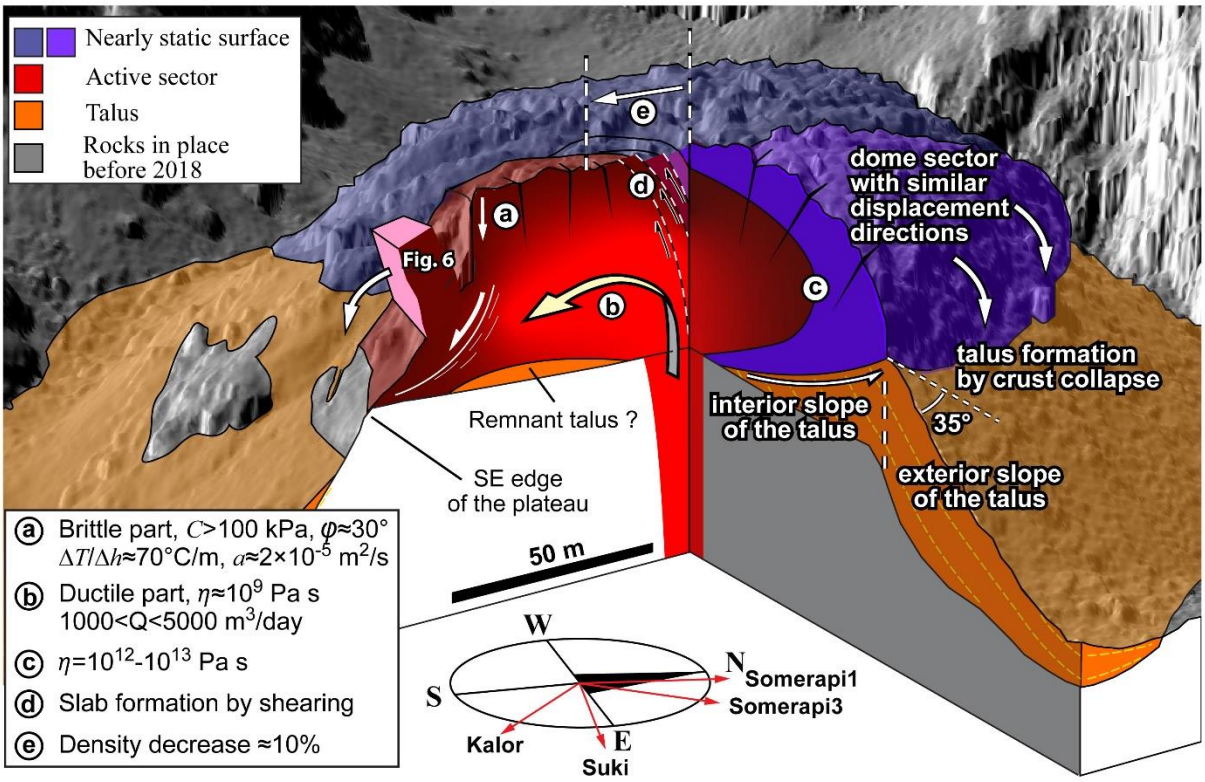


Fig. 4 Summary sketch of the observations and the interpretations of the dome emplacement (the dome morphology is that of July 2019 but some features appeared before, during phase 2 and early phase 3)

Density variations

We used the numerical code VolcFlow, which accurately simulates viscous lavas (Cordonnier et al., 2015), to simulate the dome emplacement (see section Viscosity and Fig. 7). All the simulations show a maximum thickness of the dome over the vent positions, as observed during the first weeks of growth. This morphology is also observed with other dome simulation methods (Husain et al., 2014; Harnett et al, 2018). No combination of lava rheology and effusion rate is able to reproduce the clear depression observed above the vent from October 2018 to April 2019 (and later but in an asymmetric form, Fig. 2). The simplest explanation of this central depression together with lava displacement from the vent is that the density of the lava is higher above the vent than elsewhere. This would imply an expansion of the lava in the surrounding areas by about 10% relative to the lava above the vents, over a period of a few days. Expansion could be due to gas exsolution, although no explosions were detected during this period of growth. The density change could also be caused by a bulk volume increase due to a greater abundance of cracks and faults formed by thermal contraction and brittle fracturing during movement.

Thermal properties

In September−October 2018, it took about 20 days for the lava at the surface to move from the vent to the NW collapse area (a distance of ~70 m). In the new lava front that appeared due to the collapses, the observed temperature gradient of the dome interior is about 70°C/m vertically down from the dome surface. The thermal properties can be estimated by fitting these observations to a simple conduction model. We calculated theoretical temperature gradients at 20 days using the following ranges: a dome lava thickness of 15 m to 30 m and initial temperature at the vent of 600°C to 800°C. The surface temperature is fixed at 50°C (recorded temperature) and the lava also cools by conduction into the ground. The observed gradient is reproduced with a thermal diffusivity a=1−2.5×10^{-5} m^2/s. This is at least one order of magnitude above the values for andesites and basalts (Blake and Bruno, 2000). One explanation for this could be the existence of fractures that speed up cooling by up to 10 times compared

to a homogenous lava. This fracturing is compatible with the density decrease described above and the faults observed at the surface of the dome.

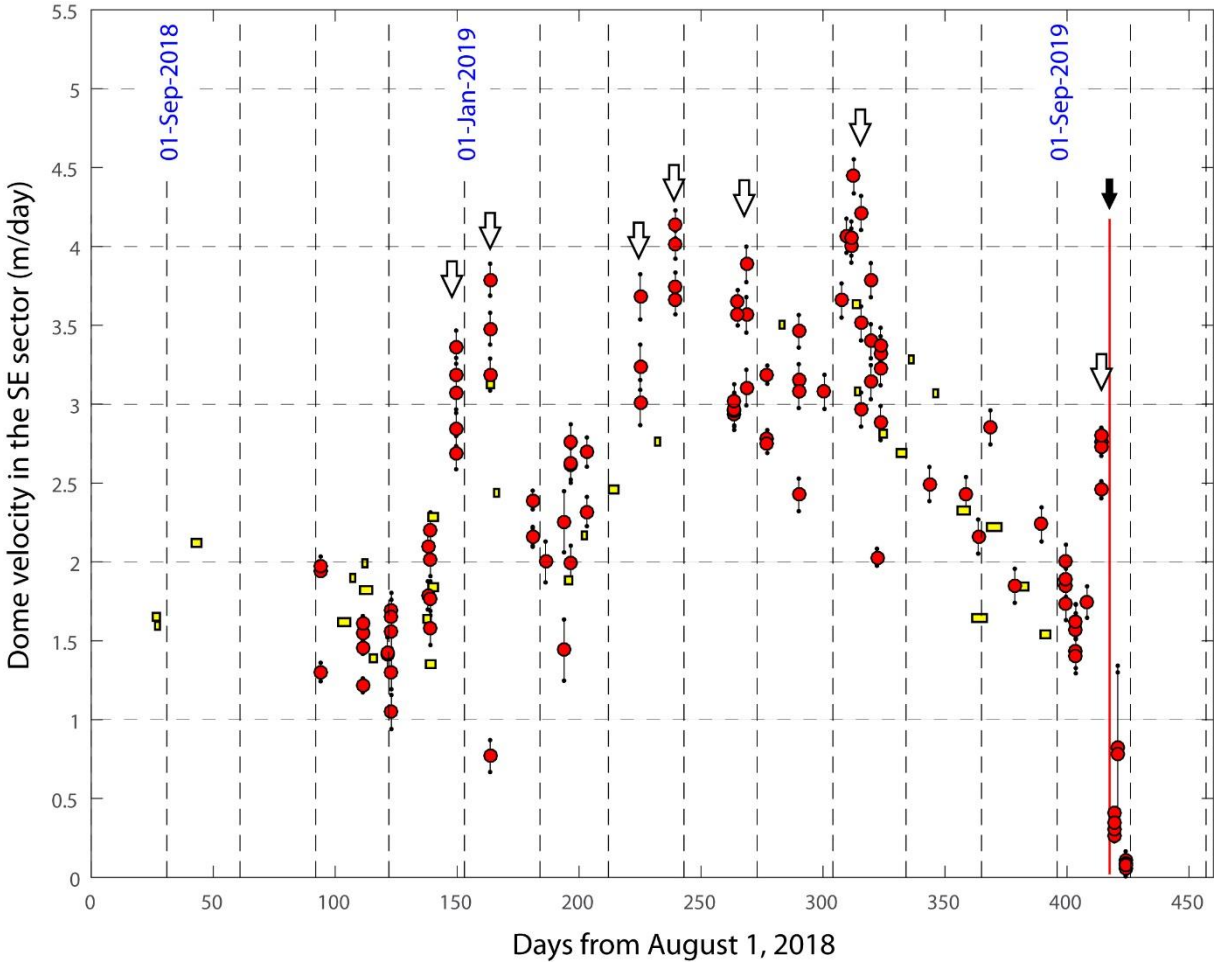


Fig. 5 Evolution of the surface velocities of the lava dome in the SE sector. The red circles are velocities calculated from visible images and the yellow rectangles from the thermal camera. The arrows indicate periods of higher flow velocities associated with a major collapse. The red line marks the explosion of 22 September 2019 and the end of the dome emplacement

Viscosity

During the first phase of the radial growth, the shape of the dome (Huppert et al, 1982), the relatively fast crustal velocity compared to the front velocity, and the absence of a talus at the front are compatible with an essentially viscous rheology. The simulations were carried out using the 2010 topography, the vent location and the effusion rate of August 2018. A Newtonian viscosity of 5×10^{10} Pa s (and a density of 2300 kg/m^3) can reproduce the front velocity of the dome (Fig. 3a) but the thickness is overestimated (22 m in the model compared to 15 m in reality). A viscosity η that increases linearly from 10^9 to 7.5×10^9 Pa s ($\eta = 10^9 \times (1 + t/2.3)$ where t is time in days) reproduces the thickness evolution observed (Fig. 3b), but the dome is too large. Moreover, the dome shape is not reproduced: the real dome is flatter than the simulation, but has a higher front. A probable explanation for this shape difference, together with the viscosity range obtained is the existence of viscosity variations; a relatively low viscosity (~ 10^9 Pa) of the hot lava near the vent would create a fairly flat dome while a higher viscosity at the front would slow down the dome's progression.

After March 2019, the activity became concentrated within a 60° sector. Although the morphology of the nearly static sectors did not evolve significantly, their surfaces continued to move slowly. From our simulations using both the dome and the talus morphologies, the mean viscosity of the NE part of the dome increased from 4×10^{12} Pa s in March to 5×10^{12} Pa s in June, 7.5×10^{12} Pa s in August and 1×10^{13} Pa s in September 2019. For the active sector, the scenario which is most compatible with both the observations and the model results is obtained using a lava viscosity of around 2×10^{10} Pa s on a 20 m thick basal layer. The upper part is a brittle crust which is just transported by the underlying lava.

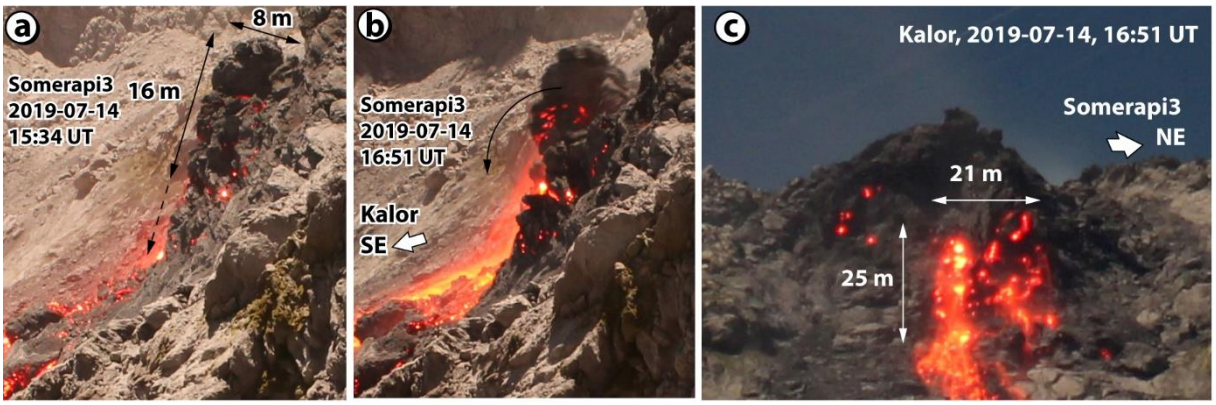


Fig. 6 Close-up photos of the front of the active lava dome showing the type of collapse that generated PDCs from December 2018 to September 2019. (a)–(b) view from a summit station. (c) view from a flank station. The front location is marked in Figure 4

Brittle behaviour and collapse

Viscous flows can become brittle at high strain rates. The viscous-brittle transition in a lava can be determined using the Deborah number $De = \eta\dot{\varepsilon}/G$ where η is the shear viscosity of the lava, $\dot{\varepsilon}$ is the strain rate, and $G = 10^{10\pm0.5}$ Pa is the elastic shear modulus of the melt (Cordonnier et al., 2012; Dingwell, 1996). The strain rate at the base of a viscous flow, where it is maximal, can be calculated by the ratio between the driving stress of the weight along the slope and the retarding viscous stress $\dot{\varepsilon} = \rho g h \sin\alpha/\eta$, where ρ is the dome density, g gravity, h is the dome thickness and α the slope. Therefore, for a lava dome, $De = \rho g h \sin\alpha/G$ is not dependant on the viscosity; a lower viscosity causes faster flow and a higher strain rate but also displaces the brittle-ductile transition to a higher strain rate. The ductile/brittle transition occurs where $De > 10^{-2}$ (Dingwell, 1996). For a 30-m-thick dome, the maximal value of $\rho g h \sin\alpha$, i.e. on a vertical slope, is ~8×10^{5} Pa. With the value of $G_{\infty} = 10^{10\pm0.5}$ (Cordonnier et al., 2012), $2.4\times10^{-5} < De < 2.4\times10^{-4}$, which is far from the value of 10^{-2}. This shows that with no stress other than its own weight, a constant-viscosity lava dome will not fracture and break up. For a real dome, the stress exerted by its more ductile core could cause the front to reach a critical *De*. However, failure does not necessarily lead to collapse as the stability after failure is that of a brittle material (this of the fractured massive lava, of the fractured crust and of the talus).

According to our observations of the 2018–2019 lava dome, the mechanism of collapse seems to be solely controlled by the slopes of the basement and the dome surface: if the slopes are less than about 35°, the dome behaves in a ductile manner and spreads out. On higher slopes, however, its behaviour is brittle. None of the collapses we observed were caused by explosions during dome emplacement (no explosion was detected by the seismic recording of BPPTKG, there were no morphological changes or ash deposited by explosion). The majority of the collapses occurred during the rainy season (November–March) but this is coincidental because the dome reached the SE edge of the plateau at the

beginning of this period (November 2018). Based on seismic signals and comparison of images of pyroclastic deposits, of the state of the dome and of the local weather, no correlation can be seen between the number or size of daily collapses, and rainfall (rainfall data in Online Resource 6). It should be noted that this conclusion does not aim to question other works that have found correlations at other lava domes.

The previous considerations indicate that collapses of the 2018−2019 lava dome obey simple laws of brittle mechanics: they occur where the stress of the dome weight exceeds the resistive stress, defined by the cohesion, the friction angle and the tensile strength of the material. The fact that the dome was not able to grow over its talus (35° slope) indicates that its friction angle - at least at its base - is also about 35° (a standard value for rocks). The dome has a very low tensile strength, probably due to the intense faulting, and cannot resist sliding. Its cohesion (estimated at 100 kPa by the height of vertical cliffs and by the size of the blocks that crumbled, Online Resource 7) enables vertical cliffs to form at the front of the active lava dome. For the previous lava domes at Merapi, cohesion can also explain the stability of steep slopes on the plateau as well the vertical cliffs that form the crater. However, due to large fractures and faults caused by shearing and thermal retraction, cohesion probably plays only a minor role in dome stability on inclined topography and at a scale of more than a few meters. The low tensile strength and cohesion, on the scale of the dome, explains why the stability of the whole lava dome appears to be controlled entirely by the angle of its base (for a basal failure) or its surface (for an internal failure). If the slopes are steeper than ~35°, the dome is in a metastable state, and can change from viscous to brittle and undergo collapse. A small increase in slope, a progressive decrease in cohesion (by cooling and thermal failure, for example), an increase in fluid pressure, high rainfall, seismic activity or an explosion could trigger a collapse that might, in any case, have been inevitable. This mechanical behaviour of the dome explains why the SE slope of the plateau, at an angle of between 40° and 50°, was an impassable obstacle for the dome growth and why the 2018−2019 lava dome was not able to expand beyond the crater.

Effusion rate, volume extruded and volume of the lava dome

The evolution of the dome and talus volumes with time provides a simple estimate of the effusion rate during Phases 1 and 2 of the dome's growth. The best results are obtained using the BPPTKG drone pictures which provide an overview of the entire dome and of the talus. Once Phase 3 began, a significant volume was removed from the summit by collapses into the Gendol valley, and the volume that accumulated at the summit tended to be constant (Fig. 8b). To estimate the volume of lava erupted, we use the velocity of the blocks at the surface of the SE sector (Fig. 4 and 5) and a numerical simulation. Detail of the calculation are given in Online Resource 7 and the code used in Online Resource 5.

The effusion rate of the lava dome is presented in Fig. 8a. The range of effusion rates is related to the range of measured velocities, which vary according to displacement disparities at the scale of each block (sliding, rotation, localised opening of fractures, etc.). Higher effusion rate can be occasionally noticed due the largest collapses that free up the lava and increase the lava velocity for a few days. Excluding these fluctuations, the general trend is a more or less linear decrease in effusion rate with time in the range defined by $Q = 4000 \pm 500 - 20/3 \times t$, where t is the time in days from 17 August 2018 (Fig. 8a). Note that this effusion rate is abnormally low for a growing dome and close to the long-term magma supply of Merapi volcano (Siswowidjoyo et al, 1995).

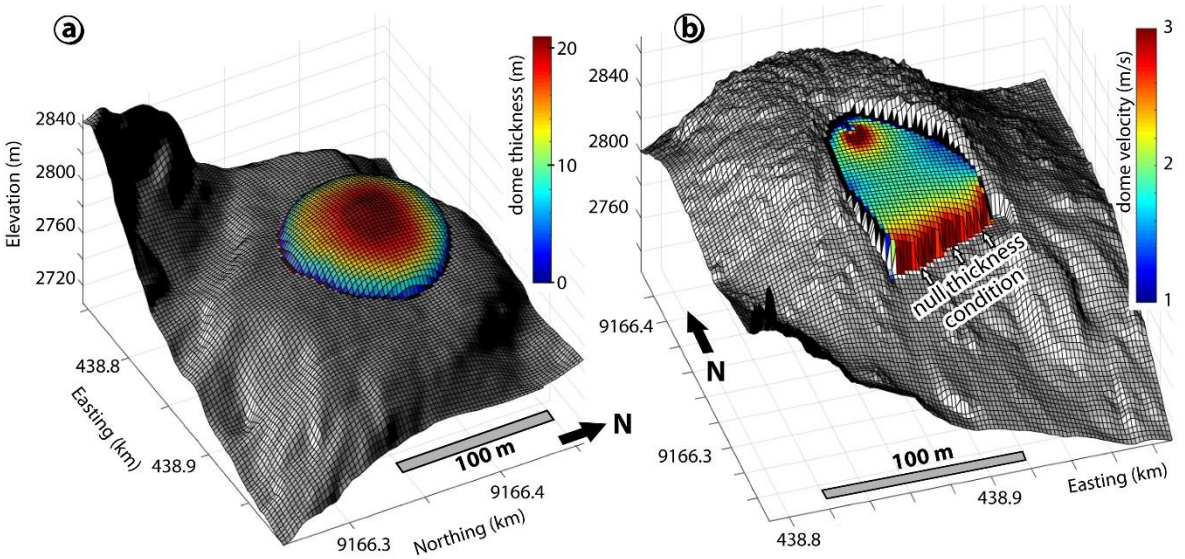


Fig. 7 Simulations of the dome emplacement with VolcFlow (a) Simulation of the 1st month on the 2010 plateau, with a viscosity of 5×10^{10} Pa s, a density of 2300 kg/m^3 and an effusion rate $Q = 4000 - 20/3\times t$ m^3/day after 30 days. (b) Simulation of the dome emplacement in the SE sector of the new dome (with a viscosity of 10^{11} Pa s, a constant effusion rate of 3000 m^3/day and a null thickness condition imposed at the front of the dome - white arrows)

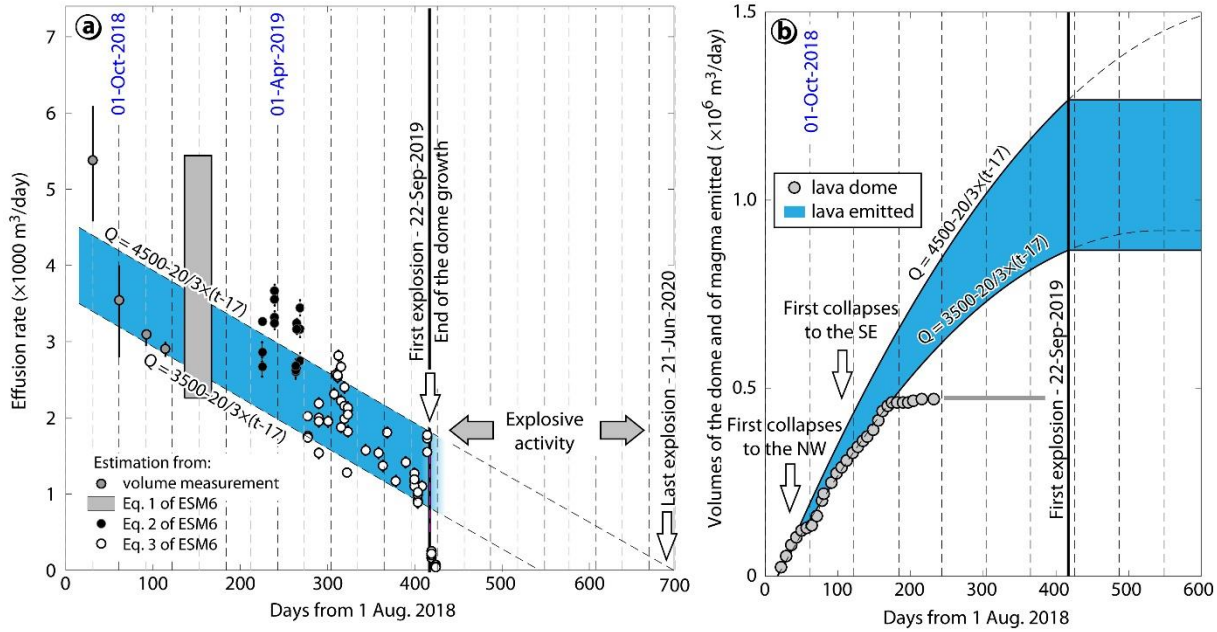


Fig. 8 (a) Effusion rate with time. The colours of the symbols are related to the method used (see ESM-7 for the equations of the effusion rates from velocities). The blue area corresponds to a linear evolution of the effusion rate between $Q = 3500 - 20/3\times t$ and $Q = 4500 - 20/3\times t$ (b) Volume of the lava dome and cumulated volume of lava emitted with time based on the equations used in (a)

By integrating the evolution of the effusion rate from August 2018 to September 2019 (when the growth stopped abruptly) we can calculate the total volume of lava emitted (Fig. 8b). This shows that the volume erupted before the end of the growth, on September 22, was between 0.85 and 1.25×10^6 m^3, while the

volume of the lava dome was less than 0.5×10^6 m^3. About twice the volume of the dome was erupted, with a volume equal to that of the final dome being lost through collapses into the Gendol valley in the form of rock falls and PDCs. Note that integrating the effusion rates after 22 September 2019 gives a volume of between 40×10^3 and 220×10^3 m^3 of lava that could have been emplaced from January to June 2020. This may explain the unusual, strong explosive activity that started at the end of dome emplacement and ended on 21 June 2020.

Dome and PDCs

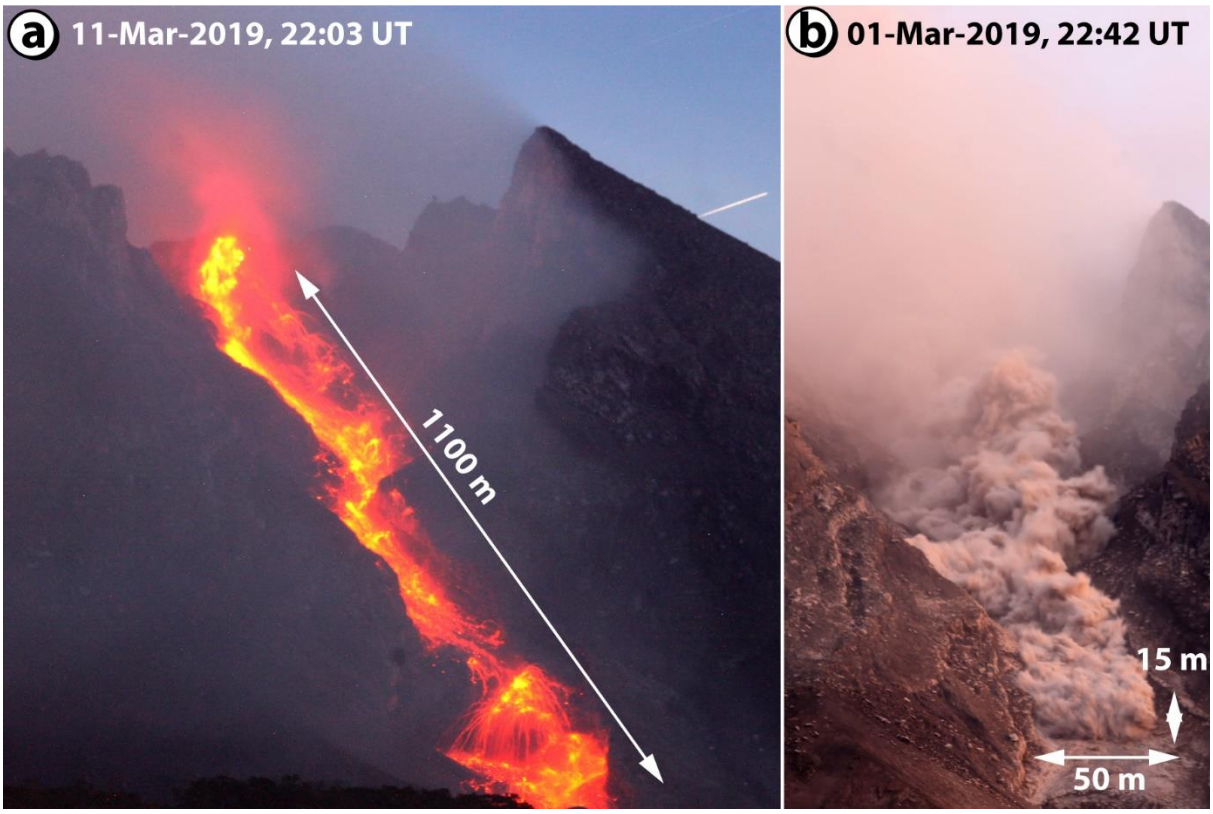


Fig. 9 (a) Pyroclastic flow recorded by night. The long duration of the exposure (600 s) makes it possible to see block trajectories through the companion ash-cloud. (b) A companion ash-cloud recorded during the day

Lava dome collapses observed during the 2018−2019 eruption resulted in the rocks bouncing, rolling, breaking up and forming rock falls or pyroclastic flows (PFs, the concentrated component of PDCs). The block trajectories were particularly visible at night (Fig. 9a). During the day, we observed the companion ash cloud or ash-cloud surge (i.e. the dilute component of the PDC, Fig. 9b). None of the PDCs travelled further than 2 km during the 2018−2019 crisis, which means that they remained on the summit cone and therefore did not pose a threat to the surrounding population.

The physics of PDCs is not well understood and the parameters that determine the runout of PFs are not fully known. However, we know that at least a critical volume is required to acquire a high fluidity and a long runout. PF deposits at Merapi, are thicker than 1−4 m (Abdurachman et al., 2000) and their width here, given the morphology of the Gendol valley, varies between 10 m and 50 m. To form a PF deposit over a distance of one kilometre from the foot of the summit cone, the volume must be greater than 10 000−200 000 m^3. In order to reach inhabited areas, it would need to be three times greater. To this volume must be added the volume that is deposited *en route* on the volcano highest slopes, between the

summit and the valley. From our observations, PFs of less than 20 000 m^3 stayed on the highest slopes. A similar value of 40 000 m^3 was found for the 1998 eruption (west flank, Schwartzkopf et al, 2005). Thus, a volume greater than 30 000 m^3 is required for a PF of 1 km, and between 50 000 m^3 and 220 000 m^3 for it to reach inhabited areas. This simple estimate is compatible with the results of Brodscholl et al. (2000) for the 22 November 1994 collapses that affected the valleys of the south flank. They estimated the volume of the PF that destroyed inhabited areas (6 km from the summit) at 260 000 m^3. Schwartzkopf et al. (2005) estimate that the volume of the PF that travelled a distance of 6 km down another valley during the 1998 collapses was between 100 000 and 500 000 m^3.

The morphology of the plateau edge forced the dome to collapse by small increments thus making it impossible to reach a critical volume on the summit slopes. If the summit topography had been different, a lava dome with an additional volume of between 0.35 to 0.75×10^6 m^3 could have developed on the SE slope of the summit. Such a volume could have generated PDCs that would have reached and destroyed inhabited areas. Therefore, the morphology of the summit, by enabling the progressive destruction of the lava dome, could explain why the 2018−2019 lava dome posed so little hazard.

Conclusion

We have developed new monitoring stations adapted to the observation of dome growth, collapses and associated PDCs. The stations were installed at Merapi volcano to track the fourteen-month growth and collapse of the 2018−2019 lava dome. The data are available online for future studies of dome emplacement and validation of numerical models.

During this period, the slopes of the dome and the underlying topography controlled the dome stability. At slopes of less than ~35° the dome emplaced as a viscous flow, while at steeper slope angles it collapsed, forming a talus or PDCs. The dome was not able to extend beyond the SE edge of the plateau and was not able to grow out of the crater. Therefore, no large collapse was possible and the summit morphology reduced the PDCs hazards. The effect of the slope on dome stability has been already noted for previous lava domes but our measurements show that the transition from stable to unstable occurs at a very limited range of slope, at around 35°. Although this needs to be confirmed by future observations for varying volumes, effusion rates and locations, real-time mapping of the summit topography could be a simple and powerful method of predicting the evolution of the hazard from future lava domes.

After five years use for observation in an aggressive environment (gas, ash, explosions, thunderstorms), the stations have proved their robustness, their autonomy, their flexibility and their adaptability. They have shown that continuous monitoring of lava dome activity is necessary to ensure our understanding of the phenomena studied. From October 2020, they are now detecting very large instabilities and displacements of several meters of half of the summit to the west, which suggest the onset of a new volcanic crisis. Such stations could be deployed on other volcanoes and other volcanic contexts to further our knowledge of hazardous or remote volcanism.

Acknowledgement

The development of the stations was funded by the *Domerapi* ANR (French *Agence Nationale de la Recherche*) Project (ANR-12-BS06-0012), the *Observatoire de Physique du Globe de Clermont-Ferrand* and the *LabEx ClerVolc* (publication number 435). The field installations and maintenance were funded by the IRD (*Institut de Recherche pour de Développement*), the project *Domerapi*, the *LabEx ClerVolc*, the Merapi Observatory (BPPTKG/CVGHM) and the Instrumented Site VELI (IRD).

The digital cameras are controlled remotely with the software gphoto2 (http://www.gphoto.org/). The camera orientations were calculated from the star positions with the software Stellarium (https://stellarium.org/fr/). The manuscript was improved by the relevant comments of two anonymous reviewers and of the Associate Editor, M. R. James.

References

Abdurachman EK, Bourdier JL, Voight B (2000) Nuées ardentes of 22 November 1994 at Merapi volcano, Java, Indonesia, J Volcanol Geotherm Res 100(1), 345−361. https://doi.org/10.1016/S0377-0273(00)00144-X

Blake S, Bruno BC (2000) Modelling the emplacement of compound lava flows. Earth Planet Sci Lett, 184, 181–197. https://doi.org/10.1016/S0012-821X(00)00278-8

Brodscholl A, Kirbani SB, Voight B (2000) Sequential dome-collapse nuées ardentes analyzed from broadband seismic data, Merapi Volcano, Indonesia. J Volcanol Geotherm Res, 100 (2000) 363–369. https://doi.org/10.1016/S0377-0273(00)00145-1

Carn SA, Watts RB, Thompson G, Norton GE (2004) Anatomy of a lava dome collapse: the 20 March 2000 event at Soufriere Hills Volcano, Montserrat. J Volcanol Geotherm Res, 100:241–264. https://doi.org/10.1016/S0377-0273(03)00364-0

Charbonnier SJ, Gertisser R (2008) Field observations and surface characteristics of pristine block-and-ash flow deposits from the 2006 eruption of Merapi Volcano, Java, Indonesia. J Volcanol Geotherm Res, 177 (4), 971−982. https://doi.org/10.1016/j.jvolgeores.2008.07.008

Cordonnier B, Caricchi L, Pistone M, Castro JM, Hess KU, Gottschaller S, Manga M, Dingwell D, Burlini L (2012) The viscous-brittle transition of crystal-bearing silicic melt: Direct observation of magma rupture and healing. Geology. 40. 611−614. https://doi.org/10.1130/G3914.1

Cordonnier B, Lev E, Garel F (2015) Benchmarking lava-flow models. Geol Soc, London. https://doi.org/10.1144/SP426.7

Darmawan H, Walter TR, Brotopuspito KS, Subandriyo, Gusti Agung Nandaka MI (2018) Morphological and structural changes at the Merapi lava dome monitored in 2012–15 using unmanned aerial vehicles (UAVs), J Volcanol Geotherm Res, 349, 256–267. https://doi.org/10.1016/j.jvolgeores.2017.11.006

Diefenbach AK, Bull KF, Wessels RL, McGimsey RG (2013) Photogrammetric monitoring of lava dome growth during the 2009 eruption of Redoubt Volcano. J Volcanol Geotherm Res, 259 308–316. https://doi.org/10.1016/j.jvolgeores.2011.12.009

Dingwell DB (1996) Volcanic dilemma-Flow or blow? Science, 273, 1054–1055, https://doi:10.1126/science.273.5278.1054

Global Volcanism Program, 2019a. Report on Merapi (Indonesia). Bull Global Vol Net, 44:4, Smithsonian Institution. https://doi.org/10.5479/si.GVP.BGVN201904-263250.

Global Volcanism Program, 2019b. Report on Merapi (Indonesia). Bull Global Vol Net, 44:10, Smithsonian Institution. https://doi.org/10.5479/si.GVP.BGVN201910-263250

Hale AJ (2008) Lava dome growth and evolution with an independently deformable talus. Geophys J Int, 174, 391–417. https://doi: 10.1111/j.1365-246X.2008.03806.x

Harnett CE, Matthew MET, Purvance D, Neuberg J (2018) Using a discrete element approach to model lava dome emplacement and collapse. J Volcanol Geotherm Res, 359, 68−77. https://doi.org/10.1016/j.jvolgeores.2018.06.017

Husain T, Elsworth D, Voight B, Mattioli GS, Jansma P (2014) Influence of extrusion rate and magma rheology on the growth of lava domes: insights from particle-dynamics modeling. J Volcanol Geotherm Res, 285:110–117. https://doi.org/10.1016/ j.jvolgeores.2014.08.013

Huppert HE, Shepherd JB, Sigurdsson H, Sparks RSJ (1982) On lava dome growth, with application to the 1979 lava extrusion of the soufrière of St. Vincent, J Volcanol Geotherm Res, 14 (3–4), 199−222. https://doi.org/10.1016/0377-0273(82)90062-2

Kelfoun K, Gueugneau V, Komorowsk JC, Aisyah N, Cholik N, Merciecca C (2017) Simulation of block-and-ash flows and ash-cloud surges of the 2010 eruption of Merapi volcano with a two-layer model. J Geophys Res, Solid Earth, 122, https://doi.org/10.1002/2017JB013981

Kelfoun K, Harris A, Bontemps M, Labazuy P, Chausse F, Ripepe M, Donnadieu F (2020) A method for 3D reconstruction of volcanic bomb trajectories. Bull Volcanol 82, 34. https://doi.org/10.1007/s00445-020-1372-z

Komorowski, J-C, Jenkins S, Baxter PJ, Picquout A, Lavigne F, Charbonnier S, Gertisser R, Preece K, Cholik N, Budi-Santoso A, Surono (2013) Paroxysmal dome explosion during the Merapi 2010 eruption: Processes and facies relationships of associated high-energy pyroclastic density currents, J Volcanol Geotherm Res, 261 (1), 260–294 Special Issue: Merapi eruption

Major JJ, Dzurisin D, Schilling SP, Poland MP (2009) Monitoring lava-dome growth during the 2004–2008 Mount St. Helens, Washington, eruption using oblique terrestrial photography. Earth and Planet Sci Lett, 286 (1–2), 243−254. https://doi.org/10.1016/j.epsl.2009.06.034

Nakada S, Zaennudin A, Yoshimoto M, Maeno F, Suzuki Y, Hokanishi N, Sasaki H, Iguchi M, Ohkura T, Gunawan H, Triastuty H (2019) Growth process of the lava dome/flow complex at Sinabung Volcano during 2013–2016. J Volcanol Geotherm Res, 382, 120–136. https://doi.org/10.1016/j.jvolgeores.2017.06.012

Newhall CG, Bronto S, Alloway B, Banks NG, Bahar I, del Marmol MA, Hadisantono RD, Holcomb RT, McGeehin J, Miksic JN, Rubin M, Sayudi SD, Sukhyar R, Andreastuti S, Tilling RI, Torley R, Trimble D, Wirakusumah AD (2000) 10,000 Years of explosive eruptions of Merapi Volcano, Central Java: archaeological and modern implications, J Volcanol Geotherm Res, 100, 1–4, https://doi.org/10.1016/S0377-0273(00)00132-3

Pallister JS, Schneider DJ, Griswold JP, Keeler RH, Burton WC, Noyles C, Newhall CG, Ratdomopurbo A (2013) Merapi 2010 eruption - Chronology and extrusion rates monitored with satellite radar and used in eruption forecasting, J Volcanol Geotherm Res, 261, 138–146. https://doi.org/10.1016/j.jvolgeores.2012.07.012

Ratdomopurbo A, Poupinet G (2000) An overview of the seismicity of Merapi volcano (Java, Indonesia), 1983–1994. J Volcanol Geotherm Res, 100, 193−214. https://doi.org/10.1016/S0377-0273(00)00137-2

Ratdomopurbo A, Beauducel F, Subandriyo J, Gusti Agung Nandaka MI, Newhall CG, Suharna, Sayudi DS, Suparwaka H, Sunarta (2013) Overview of the 2006 eruption of Mt. Merapi, J Volcanol Geotherm Res, 261, 87–97, https://10.1016/j.jvolgeores.2013.03.019

Sato H, Fujii T, Nakada S (1992) Crumbling of dacite dome lava and generation of pyroclastic flows at Unzen volcano. Nature 360, 664–666. https://doi.org/10.1038/360664a0

Schwarzkopf LM, Schmincke HU, Cronin SJ, Sheridan MF, Patra AK (2005) A conceptual model for block-and-ash flow basal avalanche transport and deposition, based on deposit architecture of 1998 and 1994 Merapi flows. J Volcanol Geotherm Res, 139 (1−2), 117−134 https://doi.org/10.1016/j.jvolgeores.2004.06.012

Siswowidjoyo S, Suryo I, Yokoyama I (1995) Magma eruption rates of Merapi volcano, Central Java, Indonesia during one century (1890–1992). Bull Volcanol, 57, 111–116. https://doi.org/10.1007/BF00301401

Sparks RSJ (1997) Causes and consequences of pressurisation in lava dome eruptions. Earth Planet Sci Lett, 150,177–189. https://doi.org/10.1016/S0012-821X(97)00109-X

Swanson DA, Dzurisin D, Holcomb RT, Iwatsubo EY, Chadwick WW, Casadevall TJ, Ewert JW, Heliker CC (1987) Growth of the lava dome at Mount St. Helens, Washington, (USA), 1981–1983, The Emplacement of Silicic Domes and Lava Flows, Jonathan H. Fink https://doi.org/10.1130/SPE212-p1

Taron J, Elsworth D, Thompson G, Voight B (2007) Mechanisms for rainfall-concurrent lava dome collapses at Soufrière Hills Volcano, 2000–2002. J Volcanol Geotherm Res, 160, 195–209. https://doi.org/10.1016/j.jvolgeores.2006.10.003

Voight B, Elsworth D (2000) Instability and collapse of hazardous gas-pressurized lava domes. Geophys Res Lett, 27 (1–4). https://doi.org/10.1029/1999GL008389

Voight B, Constantine E, Siswowidjoyo S, Torley R (2000a) Historical eruptions of Merapi Volcano, Central Java, Indonesia, 1768–1998. J Volcanol Geotherm Res, 100, 69−138. https://doi.org/10.1016/S0377-0273(00)00134-7

Voight B, Young K, Hidayat D, Subandrio, Purbawinata MA, Ratdomopurbo A, Suharna, Panut, Sayudi DS, Lahusen R, Marso J, Murray TL, Dejean M, Iguchi M, Ishihara K (2000b) Deformation and seismic precursors to dome-collapse and fountain-collapse nuées ardentes at Merapi Volcano, Java, Indonesia, 1994−1998. J Volcanol Geotherm Res, 100, 261−287. https://doi.org/10.1016/S0377-0273(00)00140-2

Walter TR, Ratdomopurbo A, Subandriyo, Aisyah N, Brotopuspito KS, Salzer J, Lühr B (2013) Dome growth and coulée spreading controlled by surface morphology, as determined by pixel offsets in photographs of the 2006 Merapi eruption. J Volcanol Geotherm Res, 261, 121–129. https://doi.org/10.1016/j.jvolgeores.2013.02.004

Online Resource

All the Online Resources, with data structured in zip files, can be downloaded at
http://opgc.fr/SO/televolc/stereovolc/data/Merapi/Codes&data.html

ESM-1: Movie of the complete growth of the 2018−2019 lava dome of Merapi volcano (Indonesia) from thermal images of Somerapi1.

ESM-2: Movie of the complete growth of the 2018−2019 lava dome of Merapi volcano (Indonesia) from visible images.

ESM-3: Additional photographs of the lava dome and the monitoring stations

ESM-4: Movie of the last weeks of the lava dome growth using anaglyphs calculated from the stereoscopic images of Somerapi1 and 3 (use blue and red glasses to see the relief).

ESM-5: Code used with the software Matlab. (1) ESM5a_viscous_profile_3D.m shows how the viscous profiles are calculated to relate the effusion rate to the surface velocities. (2) ESM5b_VolcFlow_phase1_Fig7a and ESM5c_VolcFlow_phase2_Fig7b were used for Fig. 7. They must be used with Matlab and VolcFlow. Download VolcFlow here (http://lmv.univ-bpclermont.fr/volcflow/), run VolcFlow in the command window of Matlab and load the input files. See ESM5_files_description.pdf for files description.

ESM-6: Weather data of Pasar Bubar station (mm/hour), close to the summit. The data cover the whole dome emplacement. No correlation has been identify between rainfalls and collapses.

ESM-7: Details of the calculation of the cohesion of the lava dome and of the effusion rate estimation from the measurements of the surface velocities.

Captions

Fig. 1 (a) Location of the four monitoring stations at Merapi volcano and the Gendol river. (b) 3D view of the summit before the birth of the dome, with the locations of the summit monitoring stations. The red and blue lines indicate how a point is localized in 3D by stereophotogrammetry. The red star indicates the vent location of the 2018 lava dome

Fig. 2 The three stages of the 2018−2019 lava dome growth at Merapi volcano. Left: thermal images. Right: visible images. The growth was initially radial (during phase 1, a−b), then it became asymmetric to the NW (phase 2, c−d) before forming a flow oriented to the SE (phase 3, e−f). See Online Resource 1 and 2 for a complete movie of the 14 months of growth. All the images recorded are available at the following link: http://wwwobs.univ-bpclermont.fr/SO/televolc/stereovolc/data/domerapi/Merapi.html

Fig. 3 (a) Location of the fronts of the talus (squares) and of the massive lava (circles) of the 2018−2019 lava dome over time. The locations are measured in the direction of the summit stations (N55) and of the NE edge of the plateau. Grey and white symbols are measurements to close directions (N50 and N60) to show the variability of the dome's progression. The stepped aspect of the talus curve is explained by the front progression by surface destabilisations. (b) Dome thickness with time. The red arrow indicates that the lava was lower than -6 m in the summit fissure on 10 August 2018. For both parts of the figure, the background colours identify the three phases: radial growth, anisotropic growth and oriented growth. The green lines are the results of the numerical modelling (see section on 'Viscosity')

Fig. 4 Summary sketch of the observations and the interpretations of the dome emplacement (the dome morphology is that of July 2019 but some features appeared before, during phase 2 and early phase 3)

Fig. 5 Evolution of the surface velocities of the lava dome in the SE sector. The red circles are velocities calculated from visible images and the yellow rectangles from the thermal camera. The arrows indicate periods of higher flow velocities associated with a major collapse. The red line marks the explosion of 22 September 2019 and the end of the dome emplacement

Fig. 6 Close-up photos of the front of the active lava dome showing the type of collapse that generated PDCs from December 2018 to September 2019. (a)−(b) view from a summit station. (c) view from a flank station. The front location is marked in Figure 4

Fig. 7 Simulations of the dome emplacement with VolcFlow (a) Simulation of the 1st month on the 2010 plateau, with a viscosity of 5×10^{10} Pa s, a density of 2300 kg/m^3 and an effusion rate $Q = 4000 - 20/3\times t$ m^3/day after 30 days. (b) Simulation of the dome emplacement in the SE sector of the new dome (with a viscosity of 10^{11} Pa s, a constant effusion rate of 3000 m^3/day and a null thickness condition imposed at the front of the dome - white arrows)

Fig. 8 (a) Effusion rate with time. The colours of the symbols are related to the method used (see ESM-7 for the equations of the effusion rates from velocities). The blue area corresponds to a linear evolution of the effusion rate between $Q = 3500 - 20/3\times t$ and $Q = 4500 - 20/3\times t$ (b) Volume of the lava dome and cumulated volume of lava emitted with time based on the equations used in (a)

Fig. 9 (a) Pyroclastic flow recorded by night. The long duration of the exposure (600 s) makes it possible to see block trajectories through the companion ash-cloud. (b) A companion ash-cloud recorded during the day